

**Regional Precipitation Trends 1977-2006:  
Ocean Impacts, Natural Variability and Anthropogenic Forcing**

Martin Hoerling<sup>1</sup>, Jon Eischeid<sup>1,2</sup>, and Judith Perlwitz<sup>1,2</sup>

<sup>1</sup>*NOAA/Earth System Research Laboratory, Boulder, Colorado*

<sup>2</sup>*Cooperative Institute for Research in Environmental Sciences, University of Colorado,  
Boulder, CO*

8 September 2009

Submitted to

*Journal of Climate*

## ABSTRACT

In this study, the nature and causes for observed regional precipitation trends during 1977-2006 are diagnosed. It is found that major features of regional trends in annual precipitation during 1977-2006 are consistent with an atmospheric response to observed sea surface temperature (SST) variability. This includes drying over the eastern Pacific Ocean that extends into western portions of the Americas related to a cooling of eastern Pacific SSTs, and broad increases in rainfall over the tropical eastern hemisphere including a Sahelian rainfall recovery and increased wetness over the Indo-West Pacific related to North Atlantic and Indo-west Pacific ocean warming. It is further determined that these relationships between SST and rainfall change are generally not symptomatic of human-induced emissions of greenhouse gases (GHGs). The intensity of regional trends simulated in climate models using observed time variability in greenhouse gases, aerosol, solar and volcanic aerosol forcing are appreciably weaker than observed and also weaker than simulated in atmospheric models using only observed SST forcing. The pattern of rainfall trends occurring in response to such external radiative forcing also departs significantly from observations, especially a simulated increase in rainfall over the tropical Pacific and southeastern Australia that are opposite in sign to the actual drying in these areas.

Additional experiments illustrate that the discrepancy between observed and GHG-forced rainfall changes during 1977-2006 results mostly from the differences between observed and externally-forced SST trends. Only weak rainfall sensitivity is found to occur in response to the uniform distribution of SST warming that is induced by GHG forcing, whereas the particular pattern of observed SST change that includes increased SST contrast between the east Pacific and the

Indian Ocean, and strong regional warming of the North Atlantic Ocean were key drivers of rainfall regional trends. The results of this attribution study on the causes for 1977-2006 regional rainfall changes are used to discuss prediction challenges including the likelihood that recent rainfall trends might persist.

## 1. Introduction

Regional precipitation is sensitive to sea surface temperatures (SSTs) on the interannual to multi-decadal time scale. El Niño/ Southern Oscillation (ENSO), for instance, is the main attributable cause of tropical droughts and floods that are observed interannually (e.g. Ropelewski and Halpert 1986, 1987 among many studies). A characteristic east-west dipole of Indian Ocean SST anomalies, another natural mode of coupled ocean-atmosphere variability occurring interannually, is believed to be a factor causing southeast Australian drought events (Ummenhofer et al. 2009). Decadal-long droughts and pluvials over southwestern North America and the Great Plains have also been attributed to tropical Pacific and North Atlantic SST conditions (Schubert et al. 2004a, 2004b; Seager et al. 2005), though the decade-long severity of the “Big Dry” over a large portion of Australia since 1995 appears unexplainable by Indian Ocean SST impacts alone (Ummenhofer et al. 2009). On multidecadal time scales, there is substantial evidence that much of the Sahelian drying trend during the latter half of the 20<sup>th</sup> Century resulted from slow variations in North Atlantic and Indian Ocean SSTs (e.g., Giannini et al. 2003; Hoerling et al. 2006). And key regional and seasonal features of U.S. precipitation trends during 1950-2000 have also been linked to multidecadal variability in Pacific and Atlantic SSTs (Wang et al. 2009).

Explaining the nature of regional precipitation change is key for decision makers who seek climate information to help guide their adaptation and mitigation strategies. Of particular importance is ensuring that natural variability, when occurring, is not misunderstood to indicate that climate change is either not happening or is happening more intensely than the true human

influence. Efforts to detect human influences on regional precipitation change on centennial time scales have so far been unsuccessful mainly due to a weak signal-to-noise ratio (Hegerl et al. 2007). There is some indication for the anthropogenic forcing of 20<sup>th</sup> Century changes in precipitation averaged within latitude bands (Zhang et al. 2007), perhaps related to a widening of the tropical belt (Seidel and Randel 2007; Seidel et al. 2007). However, the amplitude of 20<sup>th</sup> Century trends in zonally averaged precipitation are much larger than can be explained by an anthropogenic influence alone. An assessment by the U.S. Climate Change Science Program of the causes of North American precipitation trends during the last half-century concluded that spatial variations and seasonal differences in change were unlikely the result of anthropogenic greenhouse forcing alone, but that some of the variations likely resulted from regional SST forcing (CCSP 2009).

In this paper we diagnose the factors contributing to regional precipitation trends since the mid-1970s, a period of anthropogenic warming of the climate system as a whole that includes a substantial increase in global SSTs (IPCC 2007). We inquire whether regional precipitation trends have been consistent with SST changes, and where such associations exist, assess if they are symptomatic of natural variability and/or anthropogenic forcing. Figure 1 shows the 30-yr trend in observed annual SSTs (top) during 1977-2006 revealing a warming over most ocean basins. Conspicuous has been an absence of warming along the equatorial Pacific from the dateline to South America and an expanse of the east Pacific between 30°N and 30°S. By contrast, a relatively uniform pattern of SST warming is simulated in coupled models using observed and projected greenhouse gas (GHG) concentrations and other forcings up through 2006 (Fig. 1, middle). The diagnosis is of the Coupled Model Intercomparison Project's

(CMIP3; Meehl et al. 2007) archive of model data (which includes 22 coupled atmosphere-ocean models) using projected climate forcing changes after 1999 based on a business-as-usual scenario (A1B) that extends from the historical climate of the 20<sup>th</sup> Century runs. Our interest is not to conduct a detailed attribution of the SST changes per se (see Knutson et al. 2006; Santer et al. 2006), but rather to assess the practical implications for the differences between observed and externally forced SST changes (Fig. 1, bottom) on regional precipitation changes.

The outline of the paper and main results are as follows. Section 2 describes the data sets and methods used to diagnose causes for observed regional precipitation trends during 1977-2006. Analysis of AMIP simulations in Section 3 illustrates that major features of the observed annual precipitation trends are consistent with a SST forced signal. These include drying of the tropical east Pacific and adjacent portions of western North and South America, a recovery in Sahel rainfall, increased rainfall over the tropical Indo-west Pacific, and decreased precipitation over southeast Australia (though the latter SST signal is much weaker than the observed decline). Analysis of CMIP simulations reveals major features of observed annual precipitation trends to be mostly inconsistent with external radiative forcing. The CMIP ensemble mean yields increased rainfall over the equatorial east Pacific and southeast Australia during 1977-2006, contrary to the declines observed, whilst increased rainfall simulated over the Sahel and the tropical Indo-Pacific is an order of magnitude weaker than the observed increases. Section 3 also places the intensity of observed precipitation trends during the last 3 decades into the context of those resulting from unforced coupled ocean-atmosphere variability as well as from unforced atmosphere variability alone. Section 4 explores reasons for the substantial differences between AMIP and CMIP rainfall trends using additional climate simulations, the diagnosis of which

reveals large sensitivity to the particular pattern of SST trends and establishes that the SST trend differences seen in Fig. 1 are the main cause for their simulated rainfall trend differences.

Concluding remarks address the nature of the recent SST trends, and we pose several questions germane to predicting regional precipitation change over coming decades.

## **2. Data and Methods**

### *2.1 Observational data*

Global precipitation analysis is based on a merger of two data sets. The satellite precipitation product of the Global Precipitation Climatology Project (GPCP; Huffman et al. 1997) is used for ocean regions. These data are monthly from January 1979-present, and are gridded on  $2.5^\circ$  latitude x  $2.5^\circ$  longitude boxes. A particular strength of the GPCP product is the use of passive microwave satellite measurements which offer a more direct precipitation estimate compared to visible and infrared satellite measurements alone (WCRP 2008). The GPCP is also believed to be more realistic than the CMAP satellite product which has an artificial decreasing trend in global mean ocean precipitation (Yin et al. 2004), although one must bear in mind that existing satellite products were not specifically designed for trend analysis. The Global Precipitation Climatology Centre analysis (GPCC; Rudolf and Schneider 2005) is used for land regions.

These data are monthly from January 1901-present, and are gridded at  $0.5^\circ$  resolution.

Global monthly SST data is based the UK Meteorological Office's HadISST2  $1^\circ$  gridded analysis (Rayner et al. 2003). We also consult two other SST analyses; the  $5^\circ$  gridded Kaplan product (Kaplan et al. 2000), and the  $2.5^\circ$  gridded NOAA product (Smith and Reynolds 2005).

## 2.2 *Climate model simulations*

Two configurations of climate model simulations are used to determine the causes for observed precipitation trends; atmospheric general circulation models (AMIP), and coupled ocean-atmosphere general circulation models (CMIP). For the former, a total of 4 different models were available, each subjected to specified monthly varying observed global SSTs, but climatological values for the chemical composition of the atmosphere. An equal sized 9-member ensemble was used for each model yielding a total ensemble of 36 runs during the 1977-2006 period of analysis<sup>1</sup>. For the CMIP simulations, a total of 21<sup>2</sup> different models were utilized, each subjected to specified monthly variations in greenhouse gases, aerosols, solar irradiance and the radiative effects of volcanic activity for 1880-1999, and with the IPCC Special Emissions Scenario (SRES) A1B (IPCC, 2007) thereafter. Only a few of the modeling centers generated ensembles. To ensure equal weighting of all models, our analysis uses single runs from each of the modeling centers yielding a total ensemble of 21 members, with the model data accessed from the Program for Climate Model Diagnosis and Intercomparison (PCMDI) archive as part of the Coupled Model Intercomparison Project (CMIP3; Meehl et al. 2007). The externally forced (greenhouse gas, aerosol, solar and volcanic) signal in precipitation is estimated by averaging the multi-model CMIP ensemble members, whereas the SST-forced signal is estimated by averaging the multi-model AMIP ensemble members. The linear trend in precipitation is calculated for each model simulation, and subsequently averaged across all ensemble members.

---

<sup>1</sup> The 4 atmospheric models used are the NCAR Community Climate Model (CCM3; Kiehl et al. 1996), the NASA Seasonal-to-Interannual Prediction Project (NSIPP) model (Schubert et al. 2004a), the European Center/Hamburg model (ECHAM4.5, Roeckner et al. 1993), and the Experimental Climate Prediction Center's (ECPC) model (Kanamitsu et al. 2002).

<sup>2</sup> We did not include the MIUB-ECHO model because upper troposphere circulation data were not available for this model.

Unforced control integrations of CMIP3 coupled models are also diagnosed. Most modeling centers generated roughly 300-yr simulations using climatological well-mixed greenhouse gases associated with pre-1900 conditions. We calculate the statistics of 30-yr precipitation trends from these experiments in order estimate the influence of internal coupled ocean-atmosphere noise. Since ENSO is an important source for global precipitation variability, we select four different models that have been shown to possess realistic interannual SST variance in the tropical Pacific and also to exhibit realistic impacts on global precipitation variability (AchutaRao and Sperber 2006): the Canadian Center for Climate Modeling and Analysis CGCM3.1, the Meteorological Research Institute MRI-CGCM2.3, the National Center for Atmospheric Research PCM, and the Hadley Center for Climate Prediction and research/Met Office UKMO-HadCM3.

An additional suite of atmospheric climate model simulations are conducted that specify the 30-year change in SSTs for 1977-2006 as the sole anomalous boundary condition, with twin experiments performed that use either the observed or the CMIP SST change (see Fig. 1). We again employ four different atmospheric models, and for each generate a 30-member ensemble. The atmospheric sensitivity to the specified SST changes in these runs is determined by comparing with 50-year control integrations of each model that used a 1971-2000 climatologically averaged, seasonally varying SST.

### **3. Observed and Simulated Regional Precipitation Trends 1977-2006**

#### *a. Spatial patterns of 30-yr change*

Figure 2 compares the observed (top), AMIP simulated (middle), and CMIP simulated (bottom) trends in annual precipitation. Table 1 summarizes observed and simulated mean regional changes together with estimates for the noise of 30-yr rainfall trends. Owing to the limited availability of satellite data, the observed precipitation trends over oceans are calculated for 1979-2006, whereas the entire 30-year period beginning in 1977 is used over land. The model trends have been calculated for the entire 30-yr period over both land and oceans, and the AMIP and CMIP ensemble trends over the oceans were confirmed not to be materially different when derived for the shorter post-1979 period.

The pattern of observed precipitation change over the tropical Pacific and adjacent portions of the Americas resembles the interannual pattern associated with La Niña (Ropelewski and Halpert, 1986, 1987). A narrow band of equatorial drying is consistent with the slight cooling of the cold tongue SSTs (cf. Fig. 1). Drying fans poleward over the subtropical North and South Pacific and extends over the adjacent land areas including the southwest United States and southern Brazil. In contrast, much of the tropical eastern hemisphere experienced an increase in annual rainfall. This includes the Sahel which saw some recovery from the severe drought years of the 1970s and '80s (Lebel and Ali 2008), and much of the Indo-west Pacific region. A drying trend over eastern Australia has been a noteworthy exception to this overall regional wettening.

Diagnosis of AMIP simulations reveals that several regional features of the observed rainfall trends are consistent with the atmosphere's response to SST forcing (Fig. 2 middle). The

ensemble mean trend includes reduced rainfall over the equatorial east Pacific with drying extending into the subtropics and the western portions of the Americas. Over the eastern hemisphere, Sahel rainfall increases in response to SST variability during 1977-2006, as does rainfall over the oceanic regions of the Indo-Pacific warm pool. Only a weak precipitation response is simulated over Australia suggesting that the observed changes over that continent during the recent 30-years are not consistent with SST forcing alone.

Considerably less agreement exists between the regional patterns of observed precipitation trends and those simulated in response to external radiative forcing (Fig. 2 bottom). Notably, the amplitude of the CMIP ensemble rainfall trends is much weaker than observed, and is also weaker than in the AMIP ensemble simulations. The small amplitude compared to observations is not surprising given prior indications for a weak GHG signal-to-noise ratio for zonally averaged precipitation trends (Zhang et al. 2006).

There are several issues that may explain the different responses between AMIP and CMIP experiments. One curiosity concerns the much weaker CMIP simulated rainfall change over the Indo-west Pacific compared to AMIP, despite the fact that the CMIP SST warming trend closely approximates the observed warming in this region (Fig. 1). The general view is that tropical rainfall is sensitive to changes in SST *gradients* (for instance the large rainfall anomalies in association with the ENSO cycle during which appreciable changes in zonal SST gradients occur). We surmise that the intensity of AMIP rainfall responses over the warm pool depends not only on the local increase of the Indo-Pacific SSTs during 1977-2006, but also on the juxtaposed cooling over the eastern Pacific and the resultant increase in zonal SST contrast. In

the CMIP ensemble, there is little change in the simulated zonal SST contrast in response to GHG emissions; a relatively uniform SST warming trend occurs across the entire tropics during 1977-2006 (cf Fig. 1, bottom). Another issue is that the interannual variability of SSTs during this 30-yr period including ENSO events, which are specified in AMIP, but are unlikely to be synchronized with observations in CMIP, may also be contributing to their different rainfall trend amplitudes. In this regard, the CMIP ensemble possess additional noise that is associated with each realization's natural coupled ocean-atmosphere variability, whereas only a single SST time history evolves in the AMIP ensemble. Finally, differences in intensity of rainfall trends could also reflect limitations in the AMIP experimental design (i.e, the specification of SSTs). Each of these issues will be addressed further in section 4 using additional suites of climate simulations.

Regarding the sign of precipitation trends in response to external radiative forcing, we note the CMIP ensemble response to GHG forcing consists of increased rainfall over the equatorial Pacific, contrary to the drying observed and also contrary to the drying in AMIP simulations. Likewise, a simulated increase in east Australian rainfall is opposite to the observed drying. There is better sign agreement with the observed trends, and also with the AMIP simulated trends, over the Sahel and Indo-west Pacific warm pool (see Table 1).

*b. SST and GHG signal-to-noise ratios for 30-yr change*

Probability distribution functions (PDFs) of 30-yr trends are constructed using all individual AMIP and CMIP realizations in order to assess the roles of forcing and inherent noise in the 1977-2006 regional precipitation trends. The 30-yr change in mean-value of the PDF indicates

the SST-forced and GHG-forced signals for AMIP and CMIP populations, respectively.

Regarding the PDF spread, if our population samples had been drawn from a single model and if each realization of that model had been identically forced, then the ensemble spread of 30-yr trends would estimate the intensity of internal atmospheric noise for AMIP, and of internal coupled ocean-atmospheric noise for CMIP. The PDFs, however, are not drawn from such a homogeneous populations but from a multi-model dataset (in part to minimize biases in signal), and as such an additional factor influencing the spread is the model-dependent sensitivities to forcing. Also, individual models have not experienced identical forcing. For instance, CCM3 was forced with the Kaplan SSTs whereas ECHAM4 was forced with HadISST, and different treatments are also used for anthropogenic aerosol forcing and natural forcings among CMIP models. Our estimates of the internal noise of 30-yr trends are therefore derived not only from the PDF spreads of the multi-model samples, but also from spreads computed using ensembles of individual models that were subjected to identical boundary conditions (see Table 1).

Precipitation trends averaged for five regions that experienced considerable change are highlighted in Fig. 3. For the Pacific equatorial cold tongue region (Fig. 3a), satellite estimates indicate a -28% decline in annual rainfall, which is qualitatively consistent in sign with the drying occurring in virtually all AMIP runs (blue curve). The mean AMIP decline of -15% is statistically significant at 95%, given the outwardly small atmospheric noise contribution to 30-yr trends. By comparison, the CMIP signal (red curve) is a +10% increase, and its population sample of change is mostly inconsistent with the strong observed decline. The observed decline is also greater than that occurring in any single AMIP realization, suggesting that the observed drying intensity resulted from a combination of SST forcing and strong atmospheric noise,

though uncertainties in the satellite-derived trends and in the model sensitivities make more precise assessments difficult.

Coupled ocean-atmosphere noise is appreciably greater than atmospheric noise alone in contributing to variability of 30-year rainfall trends over the Pacific cold tongue region. This is readily apparent from a visual comparison of the AMIP and CMIP PDFs, and is further quantified in Table 1 where the spread of 30-yr trends in a multi-model average of unforced CMIP control runs is shown to be about four-fold greater than in a multi-model average of AMIP runs. This indicates that the particular evolution of observed SSTs during 1977-2006 is materially important for understanding the observed rainfall trend, and that greater uncertainty in the CMIP simulations is almost certainly due to the effect of multiple SST trajectories and the rainfall sensitivity to them. How unusual the observed 1977-2006 SST trajectory in the tropical Pacific was, and the implications for both attribution and prediction are questions addressed further in subsequent sections.

Turning attention to the eastern hemisphere warm pool region, increased rainfall over the Indo-west Pacific occurs in response to both observed SST and GHG forcing during 1977-2006 (Fig. 3d). This being one of the globe's wettest areas, the 3% of climatological increase in the AMIP ensemble mean, though modest by comparison to other regional signals, nonetheless represents a substantial total change in tropical rainfall. Further, the SST-induced wet signal is nearly triple that of the GHG-induced wet signal, which as mentioned earlier occurs despite the fact that the observed warmpool SST increase is of nearly identical strength to that occurring in the CMIP ensemble. It is plausible that the more substantial AMIP (and observed) rainfall increases could

have resulted from a sensitivity to a particular interannual behavior of warm pool SSTs, though results in section 4 will argue against such an effect for 1977-2006. Instead, it will be shown that there is a strong warmpool rainfall sensitivity to the spatial pattern of SST change across the tropical ocean as a whole. Finally, regarding the PDFs, it is interesting to note the much smaller spread among individual CMIP simulated rainfall trends over the warmpool than that occurring over the Pacific cold tongue, and further that AMIP and CMIP spreads are nearly identical over the warmpool (see Table 1). There are two primary reasons to account for this. One is that the particular observed SST trajectory specified in AMIP over the Indo-west Pacific is close to the simulated SST trajectory in CMIP occurring in response to GHG forcing. Further, owing to weak unforced interannual-to-decadal warmpool SST variability compared to that occurring in the ENSO region, individual CMIP members experienced more consistent SST evolutions from run to run owing to the strength of their coherent GHG-forced warmpool warming.

Declines in annual precipitation over southwest North America and southeast Australia have raised concern among regional water resource managers that human-induced climate change is severely degrading their water supplies, above and beyond the hydrologic consequences also being exerted by warming surface temperatures. Our diagnosis provides little support to the speculation that these dryings have been of anthropogenic origins. The CMIP ensemble does indicate a modest -8% mean decline over southwest North America during 1977-2006 (Fig. 3b). However, the amplitude of that signal is only  $\frac{1}{2}$  standard deviation of the noise in 30-yr precipitation trends associated with natural coupled variability, and there are nearly as many CMIP members yielding increased rainfall as decreased rainfall. It is therefore unlikely that the observed drying trend of -25% is due to human-induced emissions of GHGs alone. In contrast,

the AMIP ensemble signal of a -17% decline indicates that the observed drying was more consistent with variability of SSTs during the last 30-years. Importantly, 30 of the 36 AMIP simulations generate a drying trend. A relevant question is the extent to which the culpable SSTs are themselves of anthropogenic origin, and/or are attributes of natural ocean variability. Some insight comes from recalling that the Obs minus CMIP SST trend pattern resembles La Niña (Fig. 1 bottom). Figure 4 shows the observed precipitation anomalies associated with La Niña, derived by regressing annual precipitation onto an annual index of cold tongue SSTs. It is revealing that many aspects of the 30-yr observed precipitation trends over the Pacific sector and adjacent Americas are consistent with this regression pattern (cf. Fig. 2).

Neither SST nor GHG forcing appear to have contributed to the observed decline in annual precipitation over southeast Australia (Fig. 3e). In fact, the CMIP ensemble mean yields a +10% increase in annual precipitation, and the vast majority of 21 individual models show a positive trend. It is also apparent from the prior regression analysis that a reduced southeast Australian precipitation is inconsistent with a cold state of the tropical east Pacific (see also Nicholls et al. 1996). Further, in so far as both AMIP and CMIP simulations experience a similar warming of Indo-west Pacific SSTs, the Australian drying is unlikely a consequence of warmpool warming either. The observed decrease of -11% can be reconciled, however, with atmospheric internal variability alone, which according to Table 1 would require a -1.4 standardized departure event to account for the amplitude of the observed 30-yr drying.

A final regional trend of interest is the apparent recovery in Sahel rainfall (Fig. 3c). The +20% observed increase is actually exceeded by the AMIP ensemble mean trend of +25% indicating

that the recovery in Sahelian rainfall is consistent with the recent observed SST variability. This is not entirely surprising given the ability of AMIP experiments to replicate the region's rainfall trends for the 1950-1999 period (Giannini et al. 2003; Hoerling et al. 2006). The AMIP PDF is particularly skewed compared to that for other regions, the consequence of a single model whose Sahel rainfall exhibited only weak sensitivity to SSTs. Owing to this inter-model difference in signals, the atmospheric noise contribution to Sahel 30-yr trends is somewhat greater when inferred from the PDF spread of the comingled 36 AMIP runs ( $\sigma=22\%$ ) than from the spread averaged for each of the 4 models separately ( $\sigma=16\%$ , Table 1). Regarding the CMIP PDF, its ensemble mean shows only a slight Sahel rainfall increase, with nearly as many runs indicating a decrease as there are an increase. Further, the 3% ensemble mean increase pales in comparison to the estimated noise of 30-yr trends due to internal coupled ocean-atmosphere variability ( $\sigma\sim 20\%$ ), implying that even the sign of the GHG signal in Sahel rainfall change for 1977-2006 is uncertain.

#### **4. The Role of SST Trends in Regional Precipitation Changes**

The prior analysis indicates that a more realistic pattern and intensity of regional rainfall change is rendered when climate models are constrained by the trajectory of observed SST forcing than when they are constrained by the trajectory of observed GHG forcing during 1977-2006. The implication is that the particular observed SST history was critical for the observed rainfall changes, and that the differences between AMIP and CMIP simulations might be explained by their different SST forcings.

We diagnosed an additional suite of atmospheric model simulations to determine the role of the particular observed SST forcing for observed rainfall trends and we test related postulates raised previously in section 3. These model simulations were forced by the seasonal cycle of observed and CMIP ensemble SST changes for 1977-2006 period alone. In one set, an SST anomaly equal to the linear trend of observed SSTs (Fig. 1, top) have been specified, whereas the linear trend of the CMIP ensemble mean SSTs (Fig. 1, middle) has been specified in a parallel set of the same models (see section 2.2). Figure 5 shows the annual precipitation response calculated from the resulting 120-member multi-model ensemble.

One issue in section 3 was the possibility that the pattern of regional rainfall trends reflected a sensitivity to *mean changes* in SSTs, and a second issue was that a greater intensity of AMIP versus CMIP rainfall trends resulted from a sensitivity to differences in their *patterns* of SST changes. The results support a view that mean SST changes were indeed of leading importance. Much of the pattern and intensity of simulated rainfall trends occurring in AMIP and CMIP in response to time-varying forcing during 1977-2006 can be recovered by subjecting the atmosphere their 30-yr mean SST changes alone (compare Fig. 5 with the lower panels of Fig. 2).

Also evident in Fig. 5 is the appreciable sensitivity of rainfall responses to the difference between observed and CMIP mean SST changes. For instance, a tropical Pacific dry response to the observed SST trend (Fig. 5, top) contrasts with a wet response to the CMIP SST trend (Fig. 5, bottom). Recall that eastern Pacific SSTs were observed to cool during 1977-2006 versus the CMIP ensemble mean SST warming (see Fig. 1), and the results of these additional experiments

indicate that such local differences in SST change are the principal cause for differences in the AMIP versus CMIP simulated 1977-2006 Pacific rainfall trends.

Even where the local SST trends are similar between observations and CMIP simulations, such as over the Indo-west Pacific warm pool, there are appreciable differences between the rainfall sensitivities to the two specified SST changes. Note in Fig. 5 the lack of any discernable warmpool rainfall response to the CMIP SST trend but a widespread increase in rainfall to the observed SST trend. This sensitivity mimics the AMIP versus CMIP differences of Fig. 2, and suggests that the warmpool rainfall increase during 1977-2006 was linked to an *increased contrast in SSTs* between the east Pacific and warmpool region, and was not a response to local SST warming alone.

These additional experiments indicate that, at least for the 1977-2006 period, regional rainfall trends were especially sensitive to the pattern of 30-yr SST changes, and only secondarily sensitive to higher frequency components of SST variations. This is not to say that the particular temporal behavior of observed SSTs wasn't important: for example, the observed slight cooling trend of the tropical east Pacific is in part a residual of higher frequency ENSO variability. It does indicate, however, the broad linearity of precipitation responses to SST forcing, and is consistent with similar findings in Schubert et al. (2004a) regarding their diagnosis of the role of SSTs in U.S drought during the "Dust Bowl" decade of the 1930s.

A third issue raised in section 3 concerns the suitability of the AMIP approach, and to what extent the specification of SSTs in atmospheric GCMs may cause spurious sensitivity (e.g.

Kumar and Hoerling 1997). It is almost certainly not coincidental that the AMIP ensemble mean rainfall trend bears considerable resemblance to that observed, indicating that diagnosis of the atmospheric response to SSTs is a powerful tool in understanding the more complicated coupled system. But a reasonable question is to what extent the feedbacks from coupled interactions are important for understanding the precipitation trends. While a thorough answer to this question is beyond the scope of our study, some insight comes from a comparison of Figs. 2 and 5. The ensemble-mean precipitation trends simulated in the coupled CMIP models in response to GHG forcing are largely reproduced by subjecting uncoupled atmospheric models to the linear trend of the CMIP SSTs. We further note that the amplitude of rainfall responses to the specified CMIP SSTs is subdued, and is consistent with the weak amplitude occurring in the fully coupled models. This is not to discount the role of other effects that anthropogenic climate forcings (i.e. aerosols via its direct and indirect effects) included in the CMIP simulations can exert on regional precipitation changes (e.g., Ming and Ramaswamy, 2009). We are, however, reasonably assured that the AMIP ensemble precipitation trends offer a realistic diagnosis of the role of SSTs in the fully coupled observed system during 1977-2006, and that they also provide insight on the causes for rainfall trends in the CMIP simulations.

Further evidence to the SST influence is provided in Figure 6, which compares the differences in responses to the 1977-2006 observed trend versus the CMIP ensemble SST trends (left) to the maps of the trend differences between AMIP and CMIP ensemble means (right). In addition to the precipitation (top), also shown is the difference in 200 hPa height responses (bottom) which provides a dynamical framework for interpreting some of the regional precipitation differences. The outstanding feature is a wavetrain of alternating low and high pressure that arches across the

North and South Pacific Oceans that is symptomatic of the teleconnections associated with cold sea surface temperature forcing and reduced rainfall in the tropical east Pacific (cf. Fig. 4). The drier conditions over the subtropical North American and South American continent are likewise consistent with storm track shifts typically associated with such tropically forced teleconnections (e.g., Trenberth et al. 1998). Likewise, we suspect that a broad area of positive height differences extending from eastern Canada, the North Atlantic and northern Europe is associated with the greater observed warming trend of North Atlantic SSTs compared to CMIP (see Fig. 1). Indeed, a regression of annual precipitation and 200 hPa heights onto an index of North Atlantic SSTs reveals a prominent NAO-like pattern together with an increase in Sahel rainfall (not shown). The comparison between the left and right hand maps of Fig. 6 confirms that the differences between AMIP and CMIP simulations can be explained as resulting mostly from the atmospheric sensitivity to their different 30-yr SST trends. Virtually all the principal features distinguishing the AMIP from the CMIP simulated trends have their counterparts in the differences between atmospheric responses to their respective SST trends alone.

## **5. Summary and Discussion**

The nature and causes for observed regional precipitation trends during 1977-2006 have been diagnosed. We focused on a decrease in annual rainfall over the equatorial east Pacific Ocean, the subtropical north and south Pacific and adjacent western portions of the Americas. We also assessed the causes for eastern hemisphere rainfall changes including increases over the Sahel, and much of the tropical Indo-Pacific warmpool, and a notable drying over southeast Australia. Two ensemble suites of climate models were analyzed in order to determine the effect of known forcings on these regional trends in particular; the influence of GHG forcing was diagnosed from

the coupled models (CMIP3) that were done in support of the Intergovernmental Panel on Climate Change (IPCC) Fourth Assessment Report (IPCC 2007), and the influence of observed SST forcing was estimated from atmospheric models subjected to the monthly variations of global SSTs but using climatological fixed GHG concentrations.

Forcing by observed sea surface temperature variability was the principal factor explaining the pattern of regional precipitation trends during 1977-2006. The western hemisphere pattern dominated by drying was consistent with an atmospheric response to modest cooling of equatorial east Pacific SSTs, a sensitivity resembling the atmospheric response observed on interannual time scales in association with La Niña. The eastern hemisphere pattern of increased warmpool precipitation was consistent with a warming of local SSTs, and was further consistent with a sensitivity to an intensified zonal contrast of tropical SSTs during 1977-2006. Regarding recovery of Sahel rainfall, we argued that a strong warming of North Atlantic SSTs during recent decades was a leading factor. It induced a Sahelian response that is consistent with the predilection of the Atlantic ITCZ to intensify and shift poleward in concert with a warming North Atlantic (e.g. Folland et al., 1986). We found little sensitivity of Australian rainfall trends to SST forcing in our suite of AMIP models, leading to the conclusion that the southeast Australian drying in recent decades was mostly inconsistent with SST forcing.

The SST forced rainfall changes, diagnosed from AMIP simulations, was generally not symptomatic of an effect attributable to human-induced emissions of greenhouse gases. The simulated rainfall trends in CMIP simulations were found to be considerably weaker than those observed and also weaker than occurring in the AMIP simulations. Further, the spatial pattern of

GHG-induced rainfall changes differed appreciably from observations. For instance, GHG-induced increases in rainfall were simulated over the tropical Pacific and southeastern Australia contrary to observed drying in these areas. Even over the Indo-Pacific warmpool where observed and CMIP simulated SST warmings were very similar, CMIP rainfall increases were much weaker. Additional model experiments clearly reveal, however, that the discrepancy between observed and GHG-forced rainfall changes during 1977-2006 resulted mostly from the differences between their patterns of 30-yr SST change, and the atmospheric sensitivity to them. Most notably, a GHG-induced warming of the tropical east Pacific contributed to locally increased rainfall and related remote impacts in CMIP that were contrary to the effect which observed east Pacific SST cooling exerted. Overall, the pattern of uniform SST warming throughout the tropical and subtropical latitudes occurring in response to GHG forcing was found to be ineffective in inducing appreciable amplitude regional rainfall responses, whereas the observed pattern of SST change that was typified by increases in gradients was a more effective driver of regional rainfall trends.

How then are the observed changes in SSTs over the recent three decades to be understood, and how are they to be reconciled with the ocean's response to GHG-forcing? Two features of the 1977-2006 SST trend that impacted tropical rainfall trends especially were the equatorial east Pacific cooling and the warming of the Indo-west Pacific. Shown in Fig. 7 are estimates of statistical probabilities of 30-yr SST trends over these two areas, on the one hand due to the trajectory of external radiative forcing during 1977-2006 (solid curves) and on the other hand due to internal coupled ocean-atmosphere noise alone (dashed curves). The solid curves are estimates of the PDFs based on the 21 forced CMIP simulations, whereas the dashed curves are

based on 30-yr trends calculated from unforced, pre-industrial control simulations of 4 CMIP models having realistic ENSO variability (see section 2). The observed warmpool warming of  $+0.4^{\circ}\text{C}$  is equal to the mean CMIP simulated warming intensity, and significantly exceeds the spread of 30-yr trends occurring in both forced and unforced coupled models ( $\sigma\sim 0.1^{\circ}\text{C}$ ). Thus, a change in warm pool SSTs has likely been detected during the prior 30 years, one that is largely attributable to external radiative forcing (see also Knutson et al. 2006, Hoerling et al. 2004). In contrast, the observed cold tongue SSTs cooled by  $-0.1^{\circ}\text{C}$ , which was a considerable departure from the  $+0.4^{\circ}\text{C}$  mean CMIP simulated warming. No single CMIP runs generated a 30-yr cooling for 1977-2006. The large spread of 30-yr trends in the cold tongue region ( $\sigma\sim 0.2^{\circ}\text{C}$ ) could indicate though that the observed cooling resulted from a particularly strong occurrence of natural variability.

One of the important scientific issues is how the tropical oceans will respond to GHG forcing, and in particular whether the spatial pattern of change will lead to either an increased or decreased zonal contrast of SSTs between the warm pool and cold tongue regions (e.g., Vecchi et al. 2008). Clearly, the time-mean zonal SST gradient over the tropical Pacific has increased in the past 30 years, and this particular trajectory appears to be a low probability state of the CMIP ensemble simulations. The extent to which this reflects a bias in how coupled models respond to GHG forcing, whether the CMIP models underestimate the intensity of internal coupled ocean-atmosphere variability, or whether an unusual occurrence of natural variability has simply masked the GHG signal are open questions. The veracity of a particular interpretation has important implications however, since our results have shown that the particular trajectory of SSTs during 1977-2006 materially influenced the patterns of regional rainfall change, and that

significantly different regional rainfall patterns would have evolved had nature instead adopted the path of the CMIP ensemble SST change. These issues pose obvious challenges for predictions of regional rainfall change for coming decades. It is likely that mean changes in SSTs will continue to strongly influence the pattern of precipitation changes at regional scales, for instance as shown in a recent study of the joint evolution of sea surface temperature and rainfall within coupled model projections using 21<sup>st</sup> Century GHG emission scenarios (Xie et al. 2009). The challenge is predicting the SST trajectory itself, and the nascent efforts of initialized decadal forecasts (e.g., Smith et al. 2007; Keenlyside et al. 2008) will be seeking to capitalize on knowledge of the initial state of the ocean in order to render forecasts for future decades that might improve on the uninitialized projections of IPCC-type models alone.

**Acknowledgments:** We are grateful to X. Quan, T. Xu, T. Zhang for carrying out some of the experiments. This study was supported by the NOAA Climate Program Office.

## References

AchutaRao, K., and K. Sperber, 2006: ENSO simulation in coupled ocean-atmosphere modes: are the current models better? *Clim. Dyn.*, **27**, 1-15.

CCSP, 2008: Reanalysis of Historical Climate Data for Key Atmospheric Features: Implications for Attribution of Causes of Observed Change. A Report by the U.S. Climate Change Science Program and the Subcommittee on Global Change Research [Randall Dole, Martin Hoerling, and Siegfried Schubert (eds.)]. National Oceanic and Atmospheric Administration, National Climatic Data Center, Asheville, NC, 156 pp.

Folland, C., T. Palmer, and D.Parker, 1986: Sahelian rainfall and worldwide sea temperatures 1901-1985. *Nature*, **320**, 602-607.

- Giannini, A., R. Saravanan, and P. Chang, 2003: Oceanic forcing of Sahel rainfall on interannual to interdecadal time scales. *Science*, **302**, 1027-1030.
- Hegerl, G.C., F.W. Zwiers, P. Braconnot, N.P. Gillett, Y. Luo, J. Marengo, N. Nicholls, J.E. Penner, P.A. Stott, 2007: Understanding and Attributing Climate Change. Chapter 9 in *Climate Change 2007: The Physical Science Basis. Contribution of Working Group I to the Fourth Assessment Report of the Intergovernmental Panel on Climate Change* [Solomon, S., D. Qin, M. Manning, Z. Chen, M. Marquis, K.B. Averyt, M.Tignor and H.L. Miller (eds.)]. Cambridge University Press, Cambridge, United Kingdom and New York, NY, USA. 663-745.
- Hoerling, M., J. Hurrell, and J. Eischeid, 2006: Detection and attribution of 20<sup>th</sup> Century northern and southern African rainfall change. *J. Climate*, **19**, 3989-4008.
- Huffman, G.J., R.F. Adler, P. Arkin, A. Chang, R. Ferraro, A. Gruber, J. Janowiak, A. McNab, B. Rudolf, and U. Schneider, 1997: The Global Precipitation Climatology Project (GPCP) Combined Precipitation Dataset. *Bull. Amer. Meteor. Soc.*, **78**, 5–20.
- IPCC, 2007: Summary for Policymakers. In: *Climate Change 2007: The Physical Science Basis. Contribution of Working Group I to the Fourth Assessment Report of the Intergovernmental Panel on Climate Change* [Solomon, S., D. Qin, M. Manning, Z. Chen, M. Marquis, K.B. Averyt, M.Tignor and H.L. Miller (eds.)]. Cambridge University Press, Cambridge, United Kingdom and New York, NY, USA.
- Kanamitsu, M., and Co-Authors, 2002: NCEP dynamical seasonal forecast system 2000. *Bull. Amer. Meteor. Soc.*, **83**, 1019-1037.
- Kaplan, A., M. Cane, Y. Kushnir, A. Clement, M. Blumenthal, and B. Rajagopalan, 1998: Analyses of global sea surface temperature 1856-1991, *J. Geophys. Res.*, **103**, 18,567-18,589.

- Keenlyside, N., M. Latif, J. Jungclaus, L. Kornbleuh, and E. Roeckner, 2008: Advancing decadal-scale climate prediction in the North Atlantic sector. *Nature*, **453**, 84-88, doi:10.1038/nature06921.
- Kiehl, J., J. Hack, , G. Bonan, B. Boville, D. Williamson, and P. Rasch, 1998: . The National Center for Atmospheric Research Community Climate Model: CCM3. *J. Clim*, **11**, 1131-1149.
- Knutson, T., and Coauthors, 2006: Assessment of twentieth-century regional surface temperature trends using the GFDL CM2 coupled models. *J. Climate*, **19**, 1624-1651.
- Kumar, A., and M. P. Hoerling, 1998: On the specification of regional SSTs in AGCM simulations. *J. Geophys. Res.*, 8901-8907.
- Lebel, T., and A. Ali, 2008: Recent trends in the central and western Sahel rainfall regime (1990-2007). *J. Hydrol.*, doi:10.1016/j.jhydrol.2008.11.030.
- Meehl, G. , and Coauthors, 2007: The WCRP CMIP3 multimodel dataset: A new era in climate change research. *Bull. Amer. Met. Soc.*, **88**, 1384-1394.
- Ming, Y., and V. Ramaswamy, 2009: Nonlinear Climate and Hydrological Responses to Aerosol Effects. *J. Climate*, **22**, 1329–1339.
- Nicholls, N., B. Lavery, C. Frederiksen, W. Drosowsky, and S. Torok, 1996: Recent apparent changes in relationships between El Niño-Southern Oscillation and Australian rainfall and temperature. *Geophys. Res. Lett.*, **23**, 3357-3360.
- Rayner, N. A.; Parker, D. E.; Horton, E. B.; Folland, C. K.; Alexander, L. V.; Rowell, D. P.; Kent, E. C.; Kaplan, A. 2003: Global analyses of sea surface temperature, sea ice, and night marine air temperature since the late nineteenth century. *J. Geophys. Res.*, **Vol. 108**, No. D14, 4407 10.1029/2002JD002670

- Roeckner, E., and Coauthors, 1996: The atmospheric general circulation model ECHAM4: Model description and simulation of present-day climate. Max-Planck-Institute for Meteorology Rep. 218, Hamburg, Germany, 90 pp.
- Ropelewski, C., and M. Halpert, 1986: North American Precipitation and Temperature Patterns Associated with the El Niño/Southern Oscillation (ENSO). *Mon. Wea. Rev.*, **114**, 2352–2362.
- Ropelewski, C., and M. Halpert, 1987: Global and Regional Scale Precipitation Patterns Associated with the El Niño/Southern Oscillation. *Mon. Wea. Rev.*, **115**, 1606–1626.
- Rudolf, B., and U. Schneider, 2005: Calculation of gridded precipitation data for the global land-surface using in-situ gauge observations. In: *Proceedings of the 2<sup>nd</sup> Workshop of the International Precipitation Working Group (IPWG)*, Monterey, October 2004, pp. 231-247.
- Santer, B., and Coauthors, 2006: Forced and unforced ocean temperature change in Atlantic and Pacific tropical cyclogenesis regions. *Proc. Natl. Acad. Sci.*, **103**, 13905-13910.
- Schubert, S.D., M. J. Suarez, P. J. Pegion, R. D. Koster, and J. T. Bacmeister , 2004a: On the Cause of the 1930s Dust Bowl, *Science*, **33**, 1855-1859.
- Schubert, S.D., M. J. Suarez, P. J. Pegion, R. D. Koster, and J. T. Bacmeister , 2004b: Causes of long-term drought in the United States Great Plains. *J. Clim.*, **17**, 485-503.
- Seager, R., Y. Kushnir, C. Herweijer, N. Naik, and J. Velez, 2005: Modeling the tropical forcing of persistent droughts and pluvials over western North America: 1856-2000. *J. Clim.*, **18**, 4068-4091.
- Seidel, D., and W. Randel, 2007: Recent widening of the tropical belt: Evidence from tropopause observations. *J. Geophys. Res.*, **112**, D20113.
- Seidel, D., Q. Fu, W. Randel, and T. Reichler, 2007: Widening of the tropical belt in a changing climate. *Nature Geo.*, doi:10.1038/ngeo.2007.38.

- Smith, T. M., and R. W. Reynolds , 2005: A global merged land air and sea surface temperature reconstruction based on historical observations (1880-1997), *J. Clim.*, **18**, 2021-2036.
- Smith, D., S. Cusack, A. Colman, C. Folland, G. Harris, and J. Murphy, 2007: Improved sea surface temperature predictions for the coming decade from a global climate model. *Science*, **317**, 796-799, doi:10.1126/science.1139540.
- Trenberth, K. E., G. W. Branstator, D. Karoly, A. Kumar, N.-C. Lau, and C. Ropelewski 1998: Progress during TOGA in understanding and modeling global teleconnections associated with tropical sea surface temperatures, *J. Geophys. Res.*, **103(C7)**, 14,291–14,324.
- Ummenhofer, C. C., M. H. England, P. C. McIntosh, G. A. Meyers, M. J. Pook, J. S. Risbey, A. S. Gupta, and A. S. Taschetto, 2009: What causes southeast Australia's worst droughts?, *Geophys. Res. Lett.*, **36**, L04706, doi:10.1029/2008GL036801.
- Vecchi, G.A., A. Clement, and B. J. Soden, 2008: Examining the tropical Pacific's response to global warming. *EOS*. **89**, 81-83.
- Wang, H., S. Schubert, M. Suarez, J. Chen, M. Hoerling, A. Kumar, P. Pegion, 2009: Attribution of the seasonality and regionality in climate trends over the United States during 1950-2000. *J. Climate*, **22**, 2571-2590.
- WCRP, 2008: Assessment of global precipitation products. WCRP-128, WMO/TD-No. 1430, WMO, Geneva, 50pp.
- Xie, X-P., C. Deser, G. Vecchi, J. Ma, H. Teng, and A. Wittenberg, 2009: Global warming pattern formation: Sea surface temperature and rainfall. *J. Climate*, in review.
- Yin, X., A. Gruber, and P. Arkin, 2004: Comparison of the GPCP and CMAP merged gauge-satellite monthly precipitation products for the period 1979-2001. *J. Hydromet.*, **5**, 1207-1222.

Zhang, X., F.Zweirs, G. Hegerl, F.Lambert, N. Gillett, S. Solomon, P. Stott, and T. Nozawa,  
2007: Detection of human influence on twentieth-century precipitation trends. *Proc. Natl.  
Acad. Sci.*, **448**, doi:10.1038/nature06025.

**Table 1.** The 1977-2006 observed and simulated regional precipitation trends, expressed as the % change relative to observed and modeled annual climatological means. The change in means are based on the 4 model average for AMIP and the 21 model average for CMIP. The standard deviations, or noise, are based on two estimates. The first number is the spread among the 36 AMIP realizations and the 21 CMIP simulations. The number in parenthesis for AMIP is the spread among the 9-members for each model, and then averaged across the four models. The number in parenthesis for CMIP is the spread among 10 samples of 30-yr trends computed for control integrations of 4 CMIP models, and then averaged across the four models. The observed trends over the oceanic regions that comprise the cold tongue and warm pool are for 1979-2006. Figure 4 shows the geographical location of each region.

	$\Delta$ Mean (%Climo)			Std Dev (%Climo)	
	OBS	AMIP	CMIP	AMIP	CMIP
<b>Cold Tongue</b>	-28	-15	+10	6 (4)	16 (27)
<b>Warm Pool</b>	+8	+3	+1	2 (2)	2 (2)
<b>Sahel</b>	+20	+25	+3	22 (16)	20 (23)
<b>SW U.S.</b>	-25	-17	-8	21 (20)	17 (20)
<b>SE Australia</b>	-11	-1	+10	8 (8)	13 (12)

### **Figure Captions:**

**Figure 1.** The observed (top), CMIP ensemble mean simulated (middle), trends in annual sea surface temperatures during 1977-2006, and their difference (bottom).

**Figure 2.** The observed (top), AMIP ensemble mean simulated (middle), and CMIP ensemble mean simulated 30-year trends in annual precipitation during 1977-2006.

**Figure 3.** The probability distribution functions of the 1977-2006 precipitation trends occurring in the individual 36 AMIP simulations (blue PDFs), and the 21 CMIP simulations (red curve). Five regions are highlighted that experienced appreciable change in their observed precipitation during 1977-2006: (a) the equatorial Pacific cold tongue, southwest North America (b), the Sahel (c), the Indo-Pacific warm pool (d), and southeast Australia (e). Gray bands denote the geographical areas over which 30-yr precipitation trends were computed. Large gray tick on each PDF denotes the observed 30-yr change, whereas the 30-yr change for each individual AMIP (CMIP) member is denoted by blue (red) ticks.

**Figure 4.** The observed linear regression of annual precipitation (color shades) and 200 hPa heights (contours) upon an index of equatorial east Pacific SSTs for 1977-2006. The index is of the cold tongue region from 5°N-5°S, 180°-South America. Regression shown is for a -1 standardized departure of the SST index corresponding to La Niña conditions. Precipitation is % of annual climatology.

**Figure 5.** The annual precipitation response to specified SST anomalies corresponding to the 1977-2006 observed SST change (top), and the 1977-2006 CMIP ensemble mean SST change. Based on a 120-member, 4-model ensemble average. The anomalies are % of annual model climatology.

**Figure 6.** The difference in the responses to specified observed versus CMIP 1977-2006 SST changes (left). The difference between the AMIP ensemble mean simulated and CMIP ensemble mean simulated 30-year trends during 1977-2006. Precipitation (200 hPa height) differences shown on top (bottom) panels. The left panels are based on a 120-member, 4-model ensemble average. The right panels are based on the 36-member AMIP and 21-member CMIP simulations for 1977-2006. The precipitation anomalies are % of annual model climatology.

**Figure 7.** The probability distribution functions of the 1977-2006 sea surface temperature trends occurring in the 21 CMIP simulations. Two regions are shown: the Indo-Pacific warm pool (top, red curve), and the equatorial Pacific cold tongue (bottom, blue curve). The geographical areas over which 30-yr precipitation trends were computed are identical to those in Fig. 4. The probability distribution functions of 30-yr SST trends derived from pre-industrial control integrations of 4 CMIP models is superimposed in the dashed green curves. Large ticks on each PDF denotes the observed 30-yr change, whereas the 30-yr change for each individual CMIP member is denoted by small ticks.

# Annual Sea Surface Temperature Trend

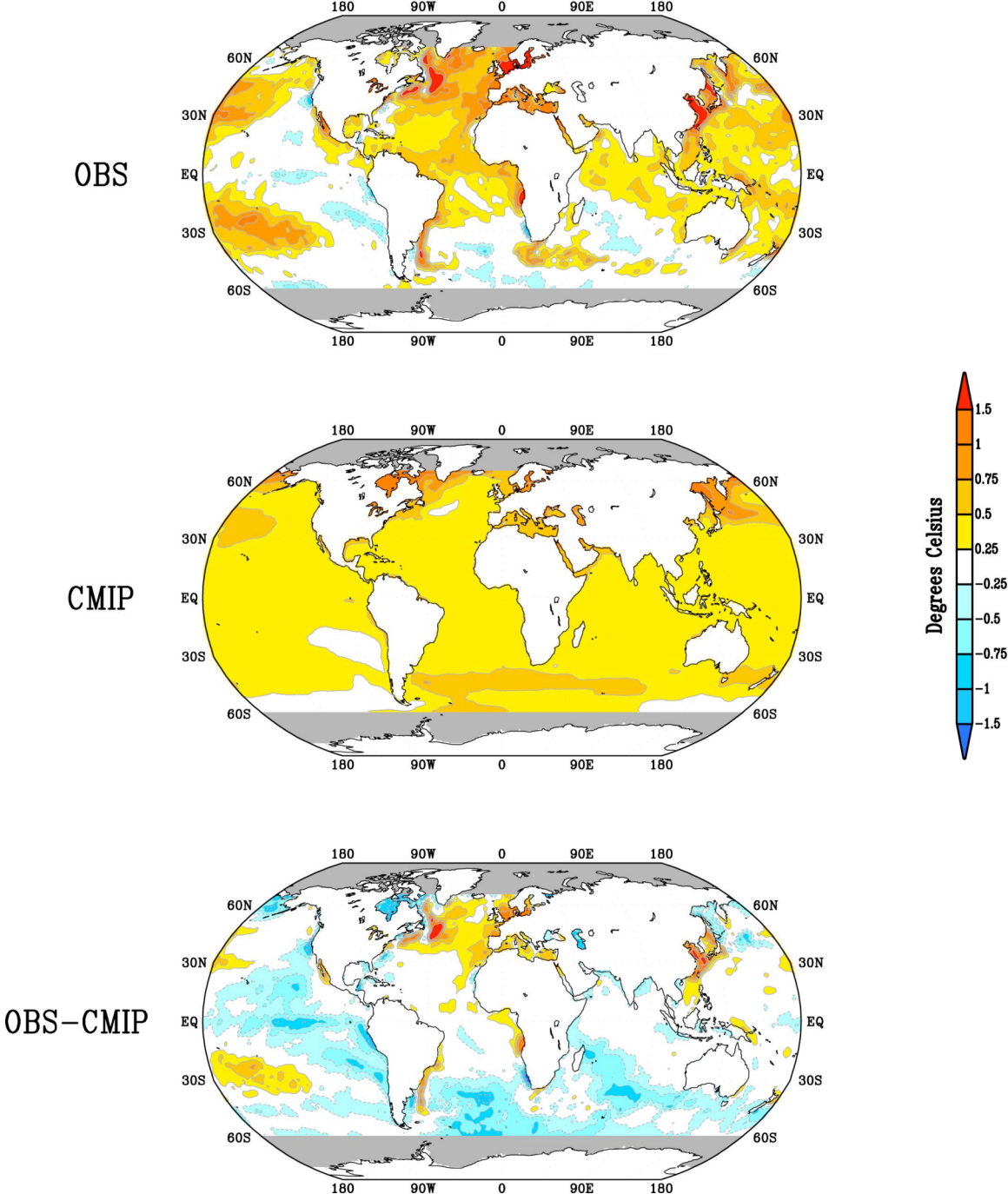


**Figure 1.** The observed (top), CMIP ensemble mean simulated (middle), trends in annual sea surface temperatures during 1977-2006, and their difference (bottom).

## Annual Precipitation Trend

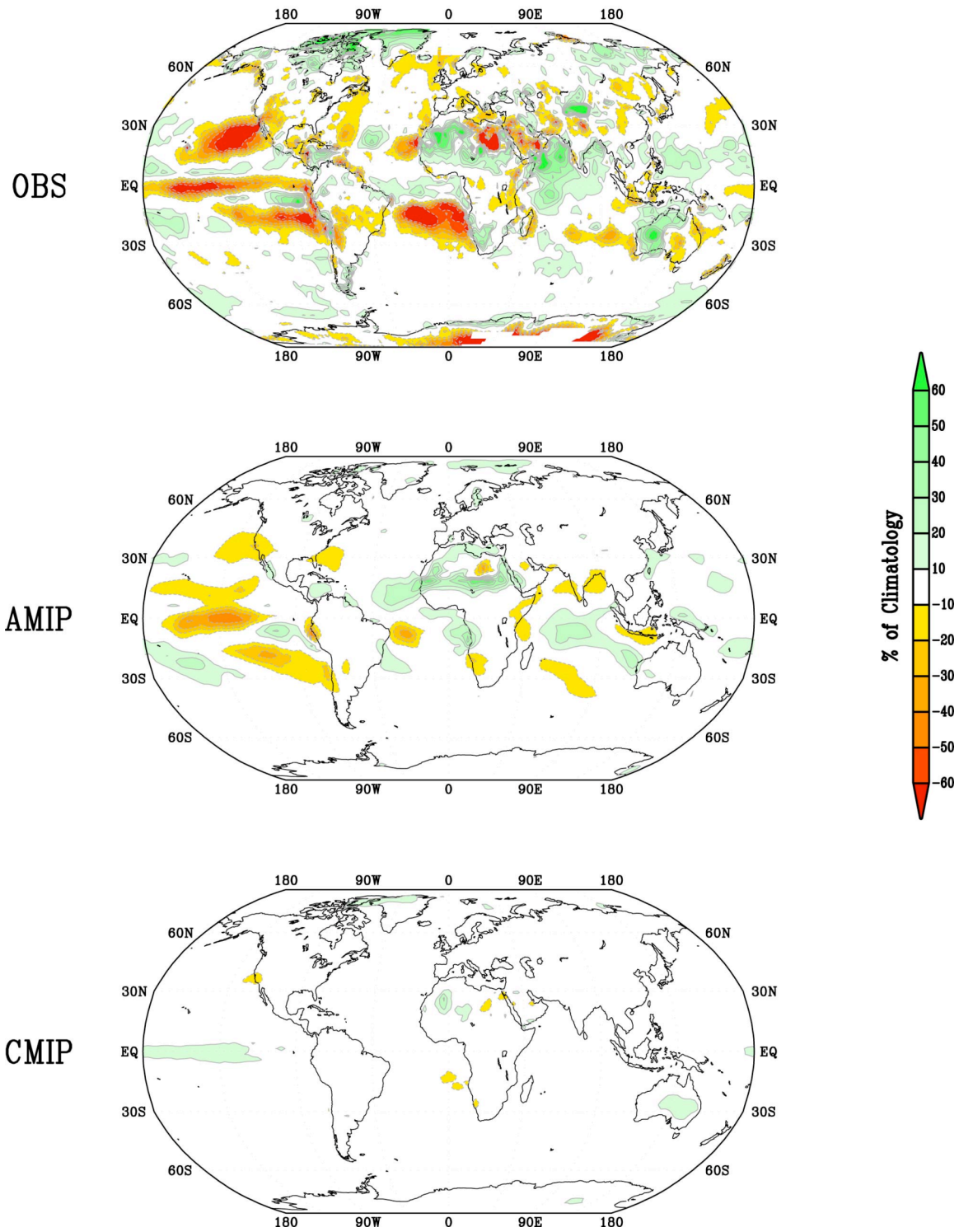


**Figure 2.** The observed (top), AMIP ensemble mean simulated (middle), and CMIP ensemble mean simulated 30-year trends in annual precipitation during 1977-2006.

Probability Distribution of Simulated Precipitation Trend  
1977–2006

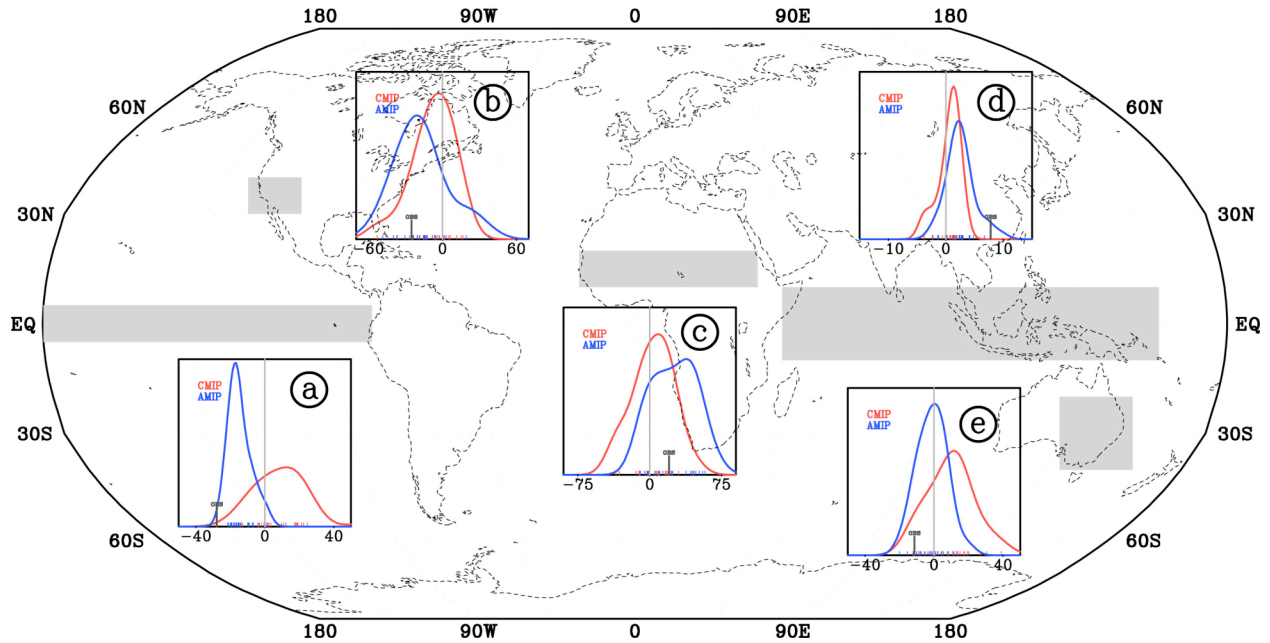


**Figure 3.** The probability distribution functions of the 1977-2006 precipitation trends occurring in the individual 36 AMIP simulations (blue PDFs), and the 21 CMIP simulations (red curve). Five regions are highlighted that experienced appreciable change in their observed precipitation during 1977-2006: (a) the equatorial Pacific cold tongue, southwest North America (b), the Sahel (c), the Indo-Pacific warm pool (d), and southeast Australia (e). Gray bands denote the geographical areas over which 30-yr precipitation trends were computed. Large gray tick on each PDF denotes the observed 30-yr change, whereas the 30-yr change for each individual AMIP (CMIP) member is denoted by blue (red) ticks.

## Cold Tongue Precipitation/200hPa Height Regressions

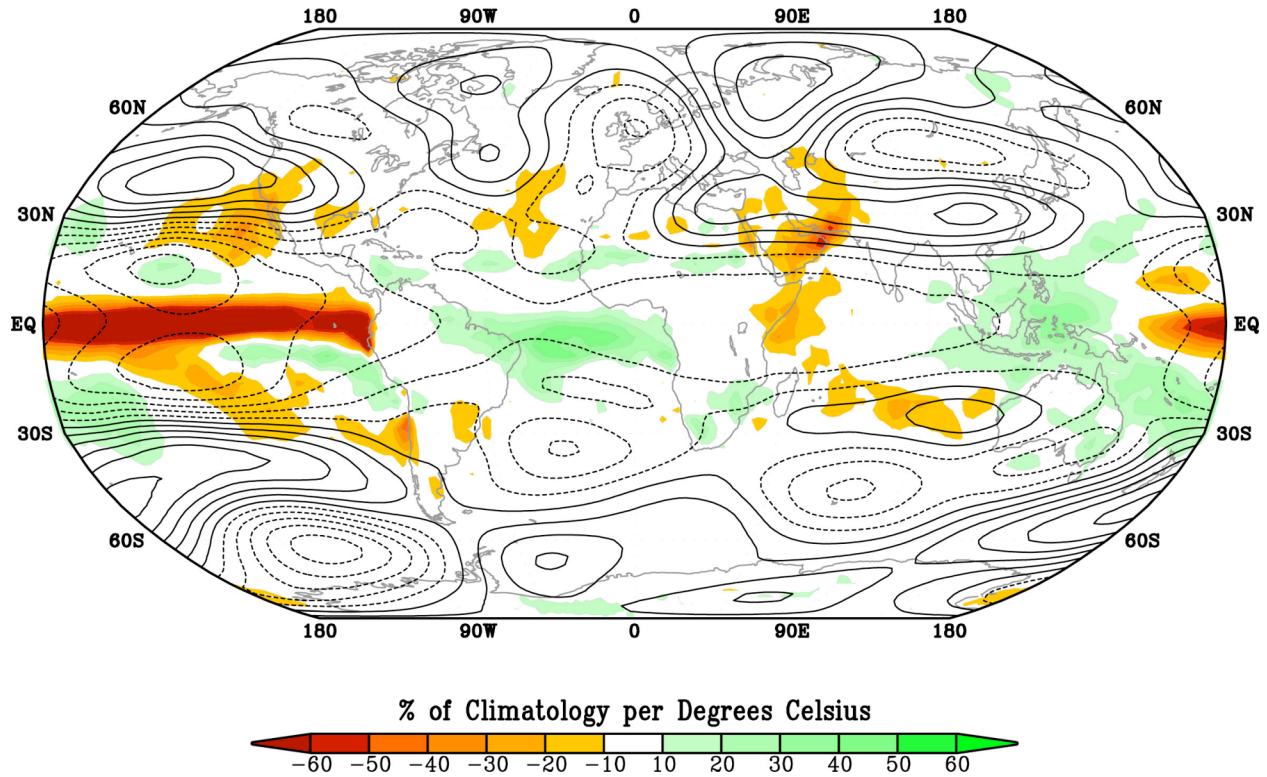


**Figure 4.** The observed linear regression of annual precipitation (color shades) and 200 hPa heights (contours) upon an index of equatorial east Pacific SSTs for 1977-2006. The index is of the cold tongue region from 5°N-5°S, 180°-South America. Regression shown is for a -1 standardized departure of the SST index corresponding to La Niña conditions. Precipitation is % of annual climatology.

## PPT Response to OBS Trend

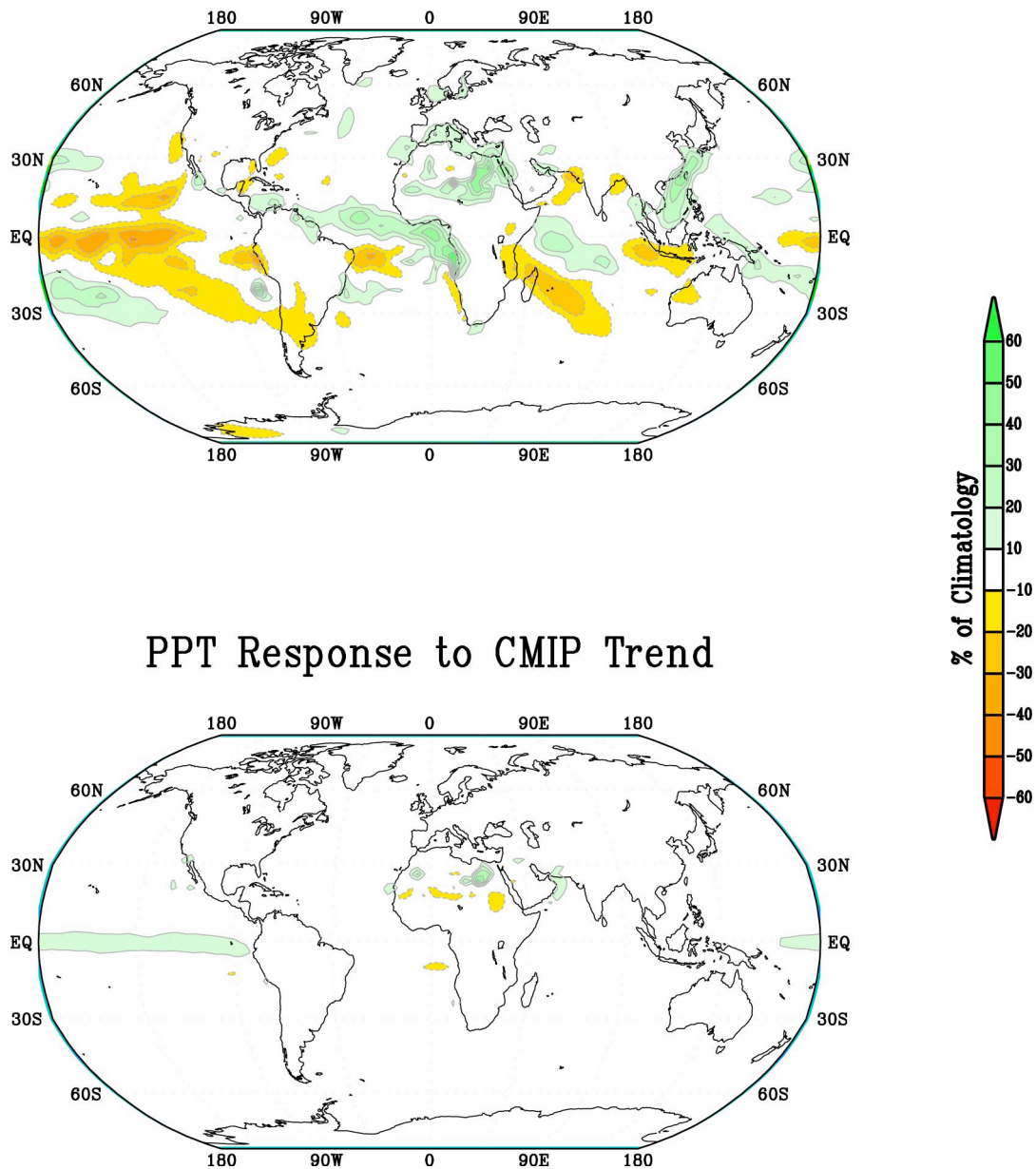


**Figure 5.** The annual precipitation response to specified SST anomalies corresponding to the 1977-2006 observed SST change (top), and the 1977-2006 CMIP ensemble mean SST change. Based on a 120-member, 4-model ensemble average. The anomalies are % of annual model climatology.

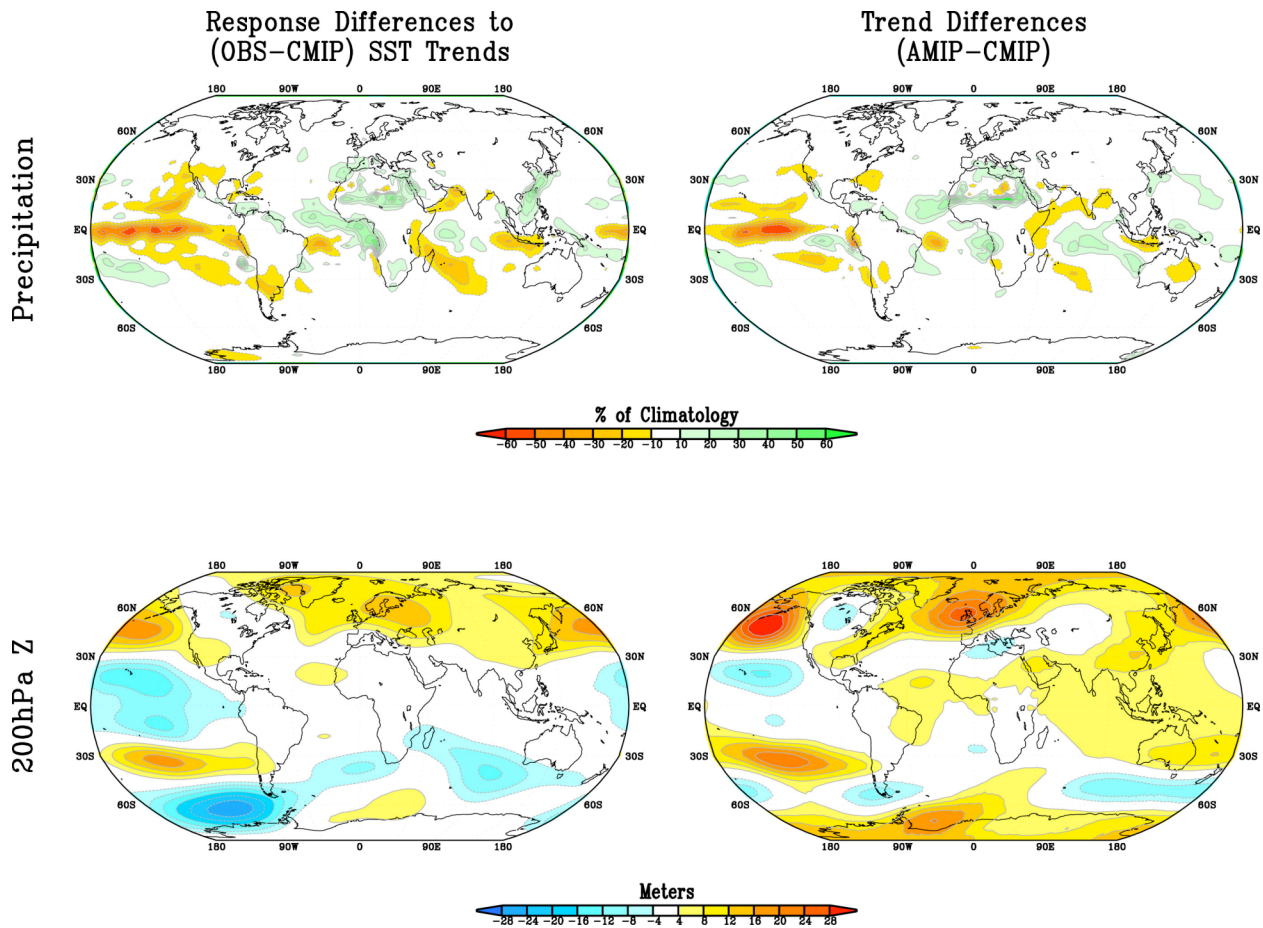


**Figure 6.** The difference in the responses to specified observed versus CMIP 1977-2006 SST changes (left). The difference between the AMIP ensemble mean simulated and CMIP ensemble mean simulated 30-year trends during 1977-2006. Precipitation (200 hPa height) differences shown on top (bottom) panels. The left panels are based on a 120-member, 4-model ensemble average. The right panels are based on the 36-member AMIP and 21-member CMIP simulations for 1977-2006. The precipitation anomalies are % of annual model climatology.

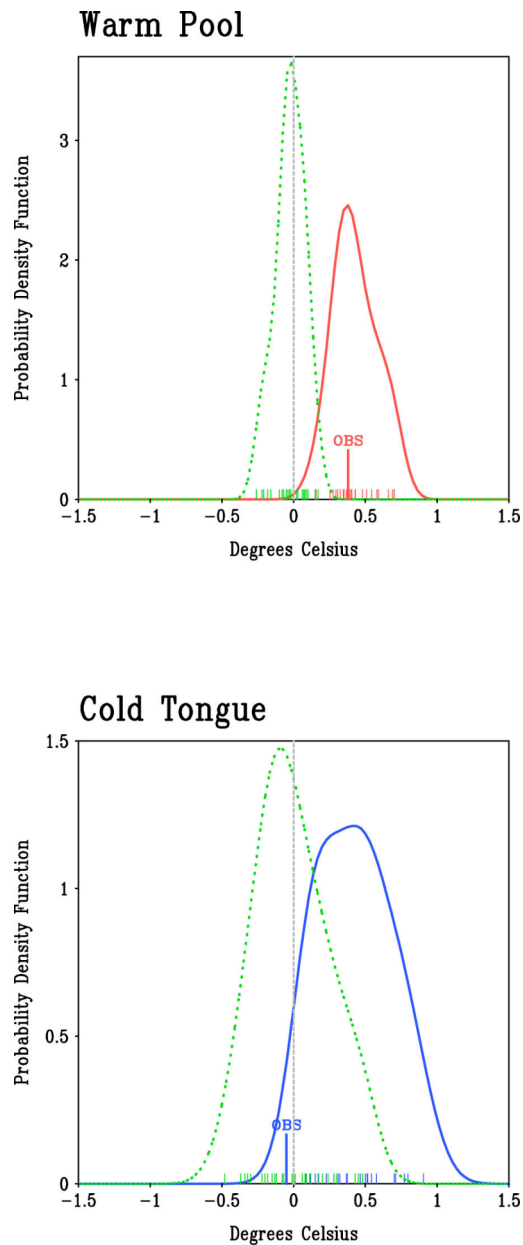


**Figure 7.** The probability distribution functions of the 1977-2006 sea surface temperature trends occurring in the 21 CMIP simulations. Two regions are shown: the Indo-Pacific warm pool (top, red curve), and the equatorial Pacific cold tongue (bottom, blue curve). The geographical areas over which 30-yr precipitation trends were computed are identical to those in Fig. 4. The probability distribution functions of 30-yr SST trends derived from pre-industrial control integrations of 4 CMIP models is superimposed in the dashed green curves. Large ticks on each PDF denotes the observed 30-yr change, whereas the 30-yr change for each individual CMIP member is denoted by small ticks.